Excess Power Gain using High Impedance and Codepositional LANR Devices Monitored by Calorimetry, Heat Flow, and Paired Stirling Engines

Mitchell Swartz
JET Energy, Inc. Wellesley, MA 02481 (USA)

Abstract — Several hundred well-controlled experiments prove that there is LANR-derived excess heat. The input power normalized delta-measurements of the LANR device and the controls confirmed that there was excess heat, as did the input power normalized heat flow measurements. The thermal waveform reconstruction calorimetry confirmed that there was excess heat. The removal of excess heat, when the LANR-driven Stirling motor was activated, eliminated the appearance of excess heat in the core. This proved that these results are not systematic instrument error.

In Phase I-II, the LANR-driven Stirling engines demonstrated power gain (over matched ohmic controls in identical calorimeters) of 170 +/-22%. The energy gain, using time-integration, was 152 +/-31%. The average electrical input power of ~3.6 watts. In Phase III-IV, the LANR-driven Stirling engines demonstrated power gain (over matched ohmic controls in identical calorimeters) to 220%. One run, with less input power to the LANR device compared to the ohmic control, gave a rotation equal to 11.6 miles for the LANR-driven engine, and 0.0 miles for the ohmic control-driven engine.

Index Terms—Optimal operating point, OOP, lattice assisted nuclear reactions, palladium, excess energy; power gain, LANR engines

1 - Introduction: LANR Propulsion Technology

Our goal has been reproducible, scalable, energy production systems of superlative heat-producing efficiency using LANR systems; maximizing electrical power gain and excess energy for propulsion to drive LANR devices. We have examined the most enthalpic of the LANR devices (Table 1) which are Pd Phusor®-type high impedance LANR devices demonstrating impressive energy gain and fairly good reproducibility [1-11]. Experiments coupled the LANR devices to LANR-driven engines (Figure 1). We report the results using LANR-driven motors, with on-line monitoring, and redundant, precision, time-resolved semiquantitative calorimetry.

Figure 1 – Stirling engines on outflow of LANR and ohmic control systems.

2.1 - Background: Lattice Assisted Nuclear reactions (LANR)

Lattice assisted nuclear reactions [LANR; 1-44] are real, and include room temperature deuterium fusion. It offers an incredibly clean, efficient potential new source of energy production. It is also free of pollution, all toxic emissions, all carbon footprints, all greenhouse gases, and radioactivity, while obviating fossil fuel. The fuel is fused deuterons, heavy hydrogen, which is plentiful in the oceans, and the product is ordinary helium in microscopic amounts. Given the prevalence of the fuel, and the incredible efficiency, LANR is an important revolutionary, potentially transformational, technology. It is a new source of energy production which emits no 'greenhouse gas', radioactivity, or toxic product. LANR can generate significant ("excess") heat in response to low energy initiation. The excess power densities range from ~7 (1989 announcement) to a reported circa 40,000W/cm^3. This magnitude of excess energy brings significant heat and even changes wrought upon the electrode. SPAWAR, JWK, Dash and others have reported volcano looking pits in electrodes. The excess energies observed with LANR are greater than any known chemical reaction, because they exceed a fraction of megajoule per day. That is important because the magnitude of this is greater than any known chemical reaction. Even if one were to replace the entire palladium cathode with TNT, one would only get 1.2 kilojoules on detonation.

2.2 - Nanostructured Materials at the Core

LANR's core are precise hydrogen-loaded alloys, nanostructured by codeposition and other methods. In successful LANR, the deuterons are packed into the metal ("loaded"), maintained, and driven by a high electric field gradient or gas pressure, with adequate incubation time, high loading, and other requisite conditions difficult to achieve. This produces a D flux in the lattice generating de novo helium and an extraordinary amount of heat. They are commensurate as Melvin Miles of China Lake has shown with Johnson-Matthey Pd rods, and Arata and Zhang reported with Zr_2O_4/Pd powder exposed to deuterium gas. The reaction is

$$D + D \text{ ----> } He^4 + \sim 22 \text{ MeV (lattice)} \quad \text{[Equation 1]}$$

The reactions are consistent with nuclear [45-50], solid state [51-57], Mossbauer [49,58-60], and radiation physics [61,10]. LANR can have both active volume and surface regions, with catastrophic desaturation capabilities [62,63]. Each location has its own, differing, rate of excess heat, tritium, and helium production and appears to be linked to a different group of optimal operating point [OOP] manifolds characterizing active LANR samples and devices [64-67]. ~10^{12} *de novo* helium are generated for every watt-second of true 'excess heat'. The helium nuclei are generated in their first excited state, and as they drop to the ground state, the lattice heats up. Although they are the dominant reactions, other branches are available under some conditions, and therefore tritium, charged particles, and neutrons can be sometimes detected.

2.3 - D-Drift Origin of Three Types of LANR

Two decades of LANR R&D have confirmed excess heat production. Today, LANR research involves electrolytic (with solution resistance ranging from conventional to 'high impedance' devices in the range of 0.2 to 0.8 megohms), gas loading, gas permeation, ion beam and glow discharge loading techniques and devices. To clarify, there are three types of so-called "electrolysis" types of LANR: conventional (F+P) and two different types of codeposition distinguished by the material onto which the deuterons are deposited (either non-D-loading or D-loading; as practiced in JET Energy and SPAWAR codeposition systems).

Deuteron, and palladium ion, drift are the reason that there exists three types of LANR. The ultimate non-equilibrium deuteron/palladium loading ratio at the surface of the palladium electrode, previously shown to depend on the loading flux minus what is lost by electrolysis [64-67], was later corrected both for intra-lattice re-diffusion of the loaded deuterons and for the secondary expected changes in electrode volume [9]. For codeposition, the coupled equations follow [see Nomenclature on p. 129 of reference 64].

$$J_{\mathrm{D}} = -B_{\mathrm{D}} * \frac{d[\mathrm{D}(z,t)]}{dz} - \mu_{\mathrm{D}} * [\mathrm{D}(z,t)] * \frac{d\Phi}{dz}$$

$$J_{\mathrm{Pd}} = -B_{\mathrm{Pd}} * \frac{d[\mathrm{Pd}(z,t)]}{dz} - \mu_{\mathrm{Pd}} * [\mathrm{Pd}(z,t)] * \frac{d\Phi}{dz}$$

[Equations 2, 3]

The mathematical solution for the time rate of change of the deuterons, palladium, and their ratio, in any given volume is determined by these fluxes and Gauss's theorem. Deuteron and palladium entry to the cathode are electron limited. Three components of the deuteron flux are considered at the cathode, again. The palladium flux at the cathode is simpler because of the absence of palladium gas formation. The mathematical solutions are determined both by the boundary conditions and by conservation of mass for both species. There is assumed conservation of deuterons with the exception of a near negligible (except with respect to product and heat) loss J_{fus} to all fusion reactions.

By assuming deriving first order reaction rates based upon the local concentrations of available material, the first-order reaction rates of deuteron loading, gas evolution and fusion (as before), and palladium deposition K_{Pd} are definable, enabling a solution, and system engineering understanding. In the steady state, the initial coefficients of the final spatial distribution are formidable, but the final result is the following paired equations.

Figure 2 demonstrates why two types of codeposition LANR and conventional LANR can be distinguished. The four curves of Figure 2 show the theoretical peak loading ratios which result from the competing processes of deuteron loading and secondary local depletion of deuterons by internal redistribution into the bulk metal. These are shown as a function of time for each of the three types of LANR systems. The lowest curve is for conventional LANR (cold fusion) electrolysis cell with LiOD as the solution. However, if the solution has too large low an electrical solution resistance, the Pd will never fill, and the D/Pd ratio will remain near zero.

The upper curves are for LANR systems where palladium cations are codeposited, along with the loaded deuterons, onto the surface of the palladium, described by Equations 2 and 3. The top curve represents codeposition upon copper, such as SPAWAR uses, and does not include redistribution within the palladium cathode. The two curves below the uppermost curve, represent slow, and then faster, internal redistribution of deuterons from the surface of the metal cathode deep into the bulk of the metal lattice. The two curves assume solution and cathode volumes of 100 and 0.5 cm^3, respectively, an electric current of 200 mA, and faradic efficiencies of 0.35 and 0.61 for palladium and deuterium, respectively. These represent the loading of Phusor®-type high impedance codeposition LANR cells [9].

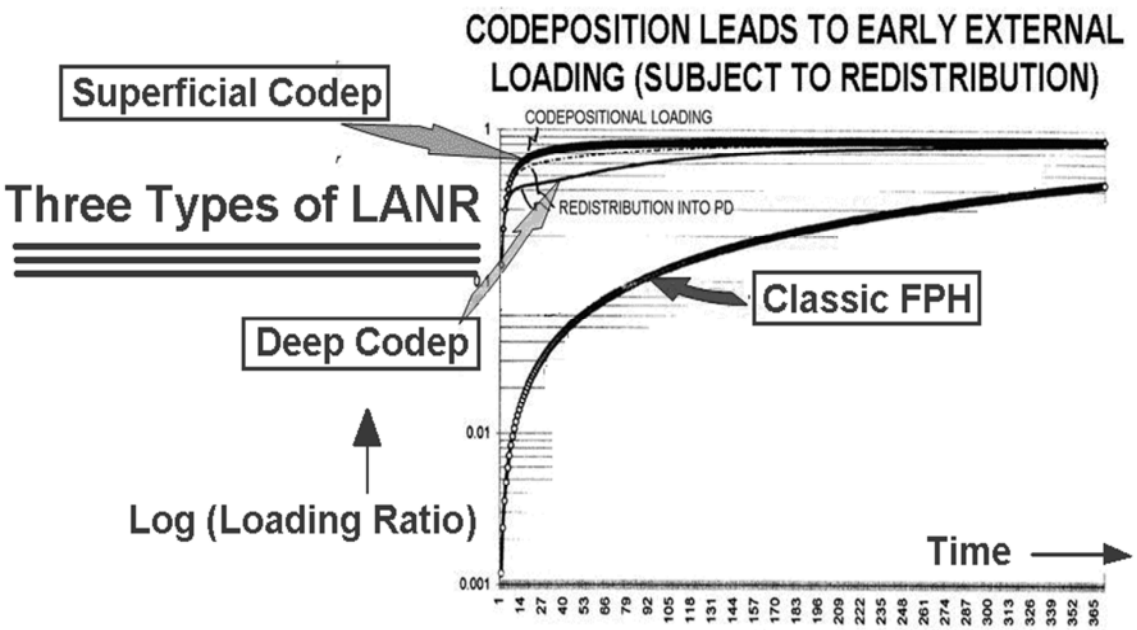

Figure 2 – Local D/Pd loading ratios for the three types of LANR systems.

3.1 – Excess Heat in LANR Systems

On one hand, development for high power has led to today's high electrical solution resistivity LANR systems (very low levels of electrolysis yield superior excess heat levels pioneered by JET Energy) and then LANR metamaterials [7]. Metamaterials use shapes engineered to control deuteron flux, even at equilibrium, and even after loading, such as shown in Figure 2. The Phusor® spiral cathode system, with its open helical cylindrical geometry, in a high electrical resistance solution, creates a unique and unusual electric field distribution. There is an anomalous effect in those portions of the cathode closest to the anode. This results in both deuteron loading flux from the solution to the electrode, and intra-palladium deuteron flux [7]. This configuration is a new kind of $Pd/D_2O/Pt$ and $Pd/D_2O/Au$ engineered LANR structure with impressive energy gain. They contain low paramagnetic content heavy water creating a unique, distinguishing electric field distribution quite different from customary wire-wire and plate-plate systems. LANR metamaterials, and high loading systems (included those explored by IENA, Energetics) and metallurgically engineered electrodes (NRL, SPAWAR, JET Energy) all point the way to high output powers and efficiencies.

On the other hand, codeposition LANR systems point the way to speedy onset for some of the reactions. Codeposition yields faster results without the prolonged incubation times. In codeposition systems, fresh Pd and D plate out together on the cathode. Highly expanded surfaces, nanoscale spherical nodules dominate on the growing surface. Deuterium loading (with an atomic ratio D/Pd>1) is obtained within seconds. The nuclear reactions occur very near the surface of the electrode (within a few atomic layers). In the original JET Energy Pd/D codeposition process, working and counter electrodes are immersed in a solution of palladium solution with neither chloride nor lithium, deposited on palladium. In the SPAWAR Pd/D codeposition process, working and counter electrodes are immersed in a solution of palladium chloride and lithium chloride in deuterated water, deposited onto silver, gold, or copper. There are physical differences in the two types involving deep diffusion [9], where Pd is deposited either on palladium (like Dr. Swartz) or upon non-loading materials such as copper, gold, silver, or platinum (like SPAWAR).

SPAWAR and JET have investigated the physical changes, the excess heat generation, hot spots with calibration showing near and far IR emission (Figure 3). JET Energy's and SPAWARS (near- and medical IR imaging) have revealed that in LANR there are cathodic hot spots, and not just Joule heating in the solution (IR drop). The desired reactions producing excess energy yield localized hot spots (Szpak). The calibrated imaging of these localized hot spots, using an infrared camera, reveal non-thermal near-IR emissions correlated with excess heat (Swartz) in active LANR devices by in situ monitoring [10]. This discovered non-thermal IR (NT-NIR) is linked, and specific, to the presence of excess heat production and not their physical temperature. This confirms the Swartz-Verner hypothesis that in LANR, unlike hot fusion, Bremsstrahlung emission, under increasingly lower temperatures, shifts from penetrating ionizing radiation toward skin-depth-locked infra-red radiation [61].

3.2 - LANR Engineering

Like hot fusion, the keys of LANR include containment, time, and density, and also flux substituted for temperature. This first key for LANR is that the PdD_x alloy must be driven, usually electrically, to extremely high loading, until it is filled and almost bursting like a sponge with water. The electrode must accept and maintain high loading for excess heat (>90%), for a sufficient incubation time, up to several hundred hours. Why? Vacancies must drift into the bulk from the surface, slightly facilitated by the loading itself [68]. The additional keys for LANR are that there must be integrity of the loaded alloy; a condition difficult to achieve, although it is circumvented to some degree by the codeposition methods, albeit with their limitations [9]. As the lattice loads, it swells. Too much swelling yields irreversible failure, like a burst balloon. Another requirement is that deuteron flux must continue, within and through the already highly loaded lattice. Efforts have continued to develop improved methods of improving output and controlling LANR kinetics, phase space, reactions, generated enthalpy and emissions. This includes a 4-14 dB gain from metamaterial technology [7], a 14-25 dB gain from Optimum Operating Point (OOP) technology [64-67]. Empirical System Identification (ESID) control may deliver an additional 10 dB improvement [69].

3.3 - Metamaterials in LANR

Metamaterials use shapes like the Phusor®-type electrode, a spiral cathode system with open helical cylindrical geometry in a high electrical resistance solution. These metamaterial shapes add properties beyond those of the material itself. In this case, the metamaterial shape is engineered to maximize deuteron flux, even after loading. In LANR, this configuration of $Pd/D_2O/Pt$ and $Pd/D_2O/Au$ devices have yielded impressive energy gain with fairly good reproducibility [1-11]. In this case, the metamaterial shape creates a unique and unusual electric field distribution involving a small region of the cathode. There is an anomalous effect in those portions of the cathode closest to the anode generating a unique, distinguishing electric field distribution quite different from customary wire-wire and plate-plate systems. This results in both deuteron loading flux from the solution to the electrode, and intra-palladium deuteron flux producing a non-equilibrium steady state condition (like a p-n junction), as is shown in Figure 3.

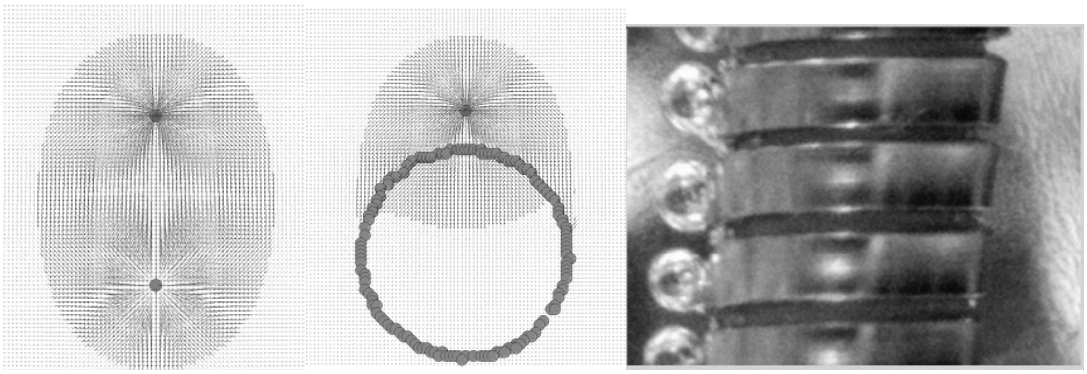

Figure 3 - Phusor LANR Cathode in High Electrical Resistance Solution
(Left) 2-D vector E-field distribution for two parallel, infinitely long, electrodes wire electrodes (anode at the top, and cathode wire).
(Middle) 2-D vector E-field distribution for the wire-PHUSOR®-type LANR system
(Right) Close-up of cathode showing asymmetric bubbling. This heralds flux through the loaded metal, which differs from how others approach the problem.

3.4 - Optimal operating point (OOP) LANR Operation

Success of LANR has been difficult to achieve because of multiple factors including significant loading, adequate confinement time (sometimes weeks), loading rate, prehistory, careful preparation, and absence of contamination and materials which quench performance. JET Energy reported that anomalous energy gain in metal deuterides became a more reproducible phenomenon as system operation was guided using continuum electromechanics. Over the years, the development of optimal operating point (OOP) technology to LANR has been one of the most useful assets in this research [JET Energy, 64-67; JWK, 70; Innoventek, 69]. Most importantly, OOP operation allows control, better understanding, more reproducible operation, and much improved success of LANR systems.

Optimal operating points, and OOP manifolds, appear when the calibrated output data of LANR device (producing amplified heat, excess power gain, de novo incremental helium-4 or tritium production) is presented as a function of the input electrical power (Figure 4). In Figure 4, three OOP manifolds are shown for LANR systems response for excess power gain, *de novo* helium and tritium production, for several LANR systems, including codeposition and palladium-black nanomaterials. The peak of each of these relatively narrow biphasic functions of LANR output production when viewed as a function along the electrical input power axis is an optimal operating point. From an operational point of view, during situations in which excess power is generated from an active LANR sample or device, large changes in LANR output, such as excess power gain, are observed as the input power is varied over a relatively small range. OOP manifold behavior is complex. They can change shape and size over weeks.

The first important point is that the OOP is that point along the input power axis where driving the LANR device yields maximum output rate of product, eg. peak excess heat, or peak helium-4 production (66,67). Thereafter, it is most important to electrically drive the devices at, or near,

their optimum operating point -- and the production of heat and He^4, or tritium, have two different OOPs which exist at two different locations along the electrical input power space. But note, the OOP peak is only one operating point at which the LANR system can be driven. The other possible operating points at which the system can be driven, are not "optimal", but are within the OOP manifold.

OOPs and OOP manifolds are universal in LANR systems, describing the generated excess heat, incremental helium-4 and tritium production for a large number, if not all, LANR systems. They are now observed to characterize Pd-heavy water LANR induced incremental helium and tritium production, and the generated excess heat production, including for conventional and high impedance $Pd/D_2O/Pt$ and $Pd/D_2O/Au$ LANR systems and Phusor®-type LANR devices, and for $Ni/H_2OD_2O_{1-x}/Pt$ and $Ni/H_2OD_2O_{1-x}$ /Au LANR devices, and for codeposition systems and codeposition LANR devices, and for tritium generated from codeposition and "FP" heavy water systems for excess heat and helium production in palladium-black systems for excess heat in light water nickel systems.

OOP Manifolds, which reflect the biphasic LANR production curves organized along the electrical input power axis, show the pathway to reproducible products, and explain a vast set of experimental data, not otherwise explicable (Figure 1). For example, OOP manifolds make salient why LANR was so difficult to achieve in the first place. Attention is directed to the simple fact that the examination of the OOP manifolds (Fig. 4) once all LANR data is thus organized formidably dispels any arguments that LANR research is not reproducible. Many negative LANR reports occur due to a failure to operate the LANR system at, or near, the optimal operating point. Driving with electrical input power beyond the peak optimal operating point (OOP) does not improve the production of the desired product, but instead yields a falloff of the production rates despite increasing input power.

OOP understanding has already proven useful to control LANR, photo-irradiation sensitivity of LANR cathodes, to maximize superior operation. OOP operation enables researchers to 'standardize' samples and devices, which has lead to several discoveries, including those which only occur when the LANR sample or device is driven at the OOP (including maximizing and controlling "heat after death", the response to incident coherent optical radiation, and non-thermal near IR emission).

The middle curve in Figure 4 is an OOP manifold which shows the excess power output (watts) observed for a heavy water deuterium-loaded Phusor-LANR and an ohmic joule control for 1 through 7 watts input electrical power. For the Phusor, the optimal operating point (OOP) is located at ~3.6 watts input power. For the Phusor, two regions of less than peak optimal output can be seen, which occur because of inadequate loading (to the left of the peak) and wasteful electrolysis (to the right of the peak). The ohmic control demonstrated "under-unity" performance and failed to demonstrate excess power gain at several different input electrical powers. The other two curves in Figure 4 show how this LANR Optimal Operating Manifold compares to two other independent investigator setups involving nanomaterials (after Arata and Zhang) and tritium (after Szpak, Gordon, Mosier-Boss).

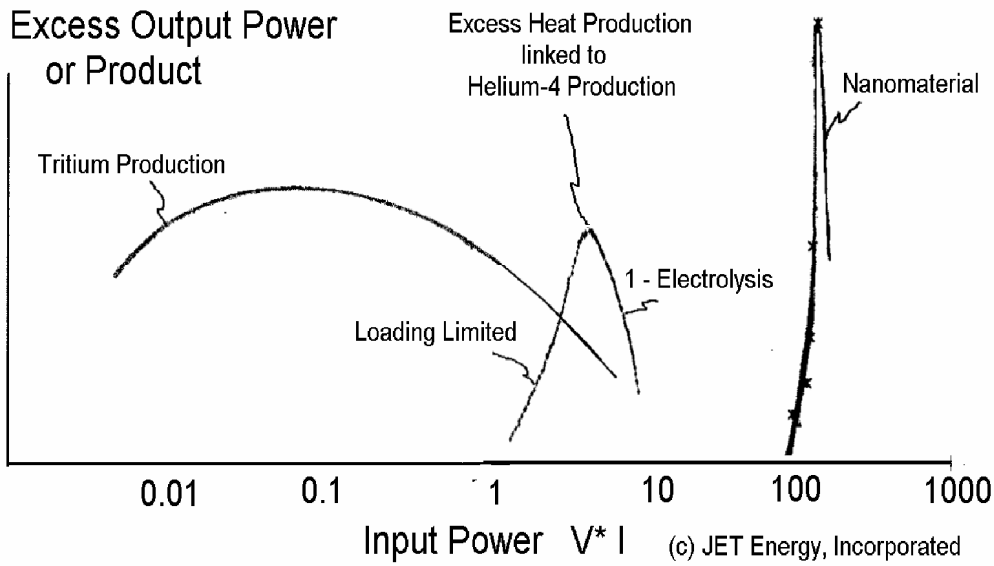

Figure 4 - Three LANR Optimal operating point (OOP) manifolds of LANR systems showing power gain and de novo helium-4 and tritium production. The central OOP Manifold is for a Pd Phusor®-type LANR device.

4.1 - Excess Heat – Experimental – Materials and Methods

As reported, in the measurement of any putative excess heat in metal deuterides, false positives must be ruled out by noise power measurement, adequate resolution Nyquist sampling, thermal waveform reconstruction, and the other techniques to obtain thermal power spectrograms. These techniques and other experimental issues including materials, loading, thermometry, calorimetry, ohmic controls to improve quality assurance, advanced paradigms to check and correct thermometry, and open circuit voltage [V_{oc}] as predictor of success, as discussed elsewhere [2].

The best modern calorimetry systems routinely employ calibration. To determine the excess energy semiquantitatively, the amount of output energy is inferred from the heat released producing a temperature rise, which is then compared to the input energy. We use calibration by at least one thermal [electrical joule control such as ohmic resistor], metallic and calorimeter control. We also routinely measure background and calorimeter noise, displaying it in "thermal power spectrograms" which also show both input electrical and derived output power, and with energy of both shown with time-integration for validation [1-11,71]. One important point here is that in all of these excess heat studies, the definition of electrical input power is $V_{input}*I_{input}$. The input energy is the time-integral of [$V_{input}(t) * I_{input}(t)$]. The excess energy, when present, is thus defined and derived as time integral of [P_{output} (t) P_{input} (t)] * t.

In these studies, there is no thermo-neutral correction in the denominator. Therefore, the observed power is a lower limit because the thermoneutral potential is usually subtracted from

the denominator, but not here. The instantaneous power gain [power amplification factor(non-dimensional)] is defined as P_{output}/P_{input}.

4.2 - Improved Semiquantitative Controlled Measurements

In this paper, we report on improved, corroboratory, redundant, and more traceable, calibrations. Some experiments now include five or more independent calorimetric and other energy-production-sensing techniques, each input-power-normalized (IPN). These are used to evaluate and help control both the excess heat and tardive thermal power (time integral is 'heat after death'). The additional calibrations now include as many of the following as possible; simultaneous redundant calorimetry, traceable heat flow sensors and measurements, corroboratory Stirling engines, down-line calorimetry measuring output around engine, corroboratory electricity or hydrogen generation, in situ observations in the visible and near-IR of the electrodes and solution, dielectric spectroscopy and transconduction measurements of the solution, and 4-terminal conductivity measurements of loaded Pd. In these peak excess energy production experiments, the heat flow is followed from the core, through heat flow measuring devices, through electricity producing devices, to paired, LANR- and ohmic control-coupled Stirling motors.

Therefore, the putative excess energy is examined by measurement of the IPN delta-T (differential temperature) at the core as a function of time, the IPN heat flow from core to the second chamber, and IPN electricity generation, IPN delta-T at the Stirling engine. This is conducted in a Dual Adjacent (DOC) Calorimetric system with a complete separate calorimeter and Stirling engine for the ohmic control, with time integration.

4.3 - Brief survey of Methods at JET Developed over Two Decades

Over two decades, our basic science research using meticulous, redundant controls, noise measurement, and time-integration (to rule out false positives) has led to the development of a new kind of clean, efficient LANR device and driving system. Success of LANR excess heat is linked to full loading, confinement time, careful preparation, absence of contamination and other issues, with performance depending upon loading rate, loading achieved, preparation of the sample, prehistory, and engineering using continuum electromechanics, beginning with the quasi-1-dimensional model of loading. Thus, there are two ways to control LANR - triggering and maintaining one optimal operating point (OOP). Successful LANR requires critical control of input power, the OOPs of the driven systems, loading (> 85-90%), and loading flux. Worse, the driving and loading fluxes needed for the reactions have a side effect. They can easily destroy a Pd specimen making it never work again. This occurs because there are complex metallurgical problems which involve swelling grain size and changing orientations, occurring at increased loadings, deforming the lattice.

More than 1 gigapascals pressure produces stress, strain, cracks, deloading, and the usual "fatal" cracking. Therefore, again, perhaps most important has been driving the devices at their optimum operating point for peak excess heat production points along the input electrical power axis, where each are maximized, respectively, with minimal solution electrical conductivity, free of contamination and materials which quench performance.

LANR can generate significant ("excess") heat in response to low energy initiation. We reported the incremental impact of red laser irradiation on Pd LANR cathodes, and reported that part of the impact is due to reflection off of the cathode back into the double layer. There, deuteron injection into the palladium increases (activation energy of ~14 kilocalories per mole) from microwave rotation and IR vibration for the intermolecular transfer of deuterons to the Pd [8]. The impact is that "paradoxically" (unless considered this way), although the excess heat increases, the power gain falls. Hagelstein, Letts and Cravens [19] have also reported both single and dual photon impacts on cathodes. The important point is that several types of experiments have revealed that input energy levels of less than 10eV (involving the applied electric field, with or without additional visible light irradiation) can successfully stimulate production of excess heat of megajoules and, on occasion, stimulate nuclear by-products, including neutrons which have been detected at energies exceeding 12 MeV [27].

This report goes further than any other in the past, with new measurements including multiple independent sensing techniques, each input normalized to input power. The evaluations now include corroboratory measurements made by up to 6 independent, different methods to evaluate the presence, if any, of excess heat, redundant calorimetry, and traceable heat flow sensors. Improved corroboratory measurements now include five or more independent calorimetric or other sensing techniques, each input-power-normalized, to evaluate, and certify possible anomalous heat.

5.1 - High Impedance JET Energy PHUSORS

JET Energy has shown that some electrodes, of specific shape, are metamaterials which produces excess heat of a superlative magnitude, successfully driving Stirling engines at the 1-19+ watt level. The control of LANR by precise, prolonged material fabrication, metamaterial shape selection, control of D-flux and post D-loading flux, are key for efficient energy production. In the most efficient systems a high impedance (High-Z) Phusor®-type LANR Device was used with low electrical conductivity D_2O, and no additional electrolyte. This bathes the metamaterial shaped spiral cathode.

The Pd Phusor®-type high impedance LANR devices have shown impressive energy gain and fairly good reproducibility. High impedance LANR devices include nickel and palladium high electrical impedance Phusor [$Pd/D_2O/Pt$, $Pd/D_2O/Au$, $Pd(Ti\text{-}coupled)/D_2O/Pt$, $Ni/H_2O_{1-x},D_2O_x/Pt$, $Ni/H_2O_{1-x},D_2O_x/Au$], and some codepositional DAP-[$Pd/Pd(OD)_2/Pt$] LANR devices. These high impedance LANR devices have shown power gains 200% to 400%, and to ~8000% power gain for a short time for one DAP Phusor®-type, compared to input energy and to input energy transferred to conventional dissipative devices. In 2003, we demonstrated a working Pd primitive Phusor®-type high impedance LANR system for five days at MIT at ICCF-10. It produced ~230% power gain at 1 to 2 watt level, compared to thermal control, while demonstrating optimal operating point operation. Other, more robust, devices have enabled some LANR-driven motor engineering of Stirling engines at the 1-19+ watt levels, and higher for short times, and lower efficiencies.

The output of some LANR devices are shown in Figures 5 through 11, and in Table 1. Representative time histories (Figures 5 and 6) show both input and output electrical powers and energies. The input electrical power was switched manually between the LANR device and the resistor ("Control"). Integrated total energy for electrical input (solid red line) and thermal output (dashed blue line) are shown. The total input energy over 4000 minutes is illustrated by the solid red line, giving a result near 480 kJ. The total output energy over 4000 minutes is illustrated with the dashed blue line, giving a result of about 820 kJ. One observes in this run an energy gain of 1.7. The data marked by "PHUSOR" represents the nanostructured LANR sample and heralds electrical power supplied to it. An excess heat is induced at low power with a gain near 200%, after which the system is taken to higher input power, where the power gain is lower, near 130%, followed by another calibration pulse. After this, the cell produces excess heat under varying conditions. Two additional curves, the result of time-integration, on Figure 5 support the excess heat of the deuterium-loaded palladium system compared to the control.

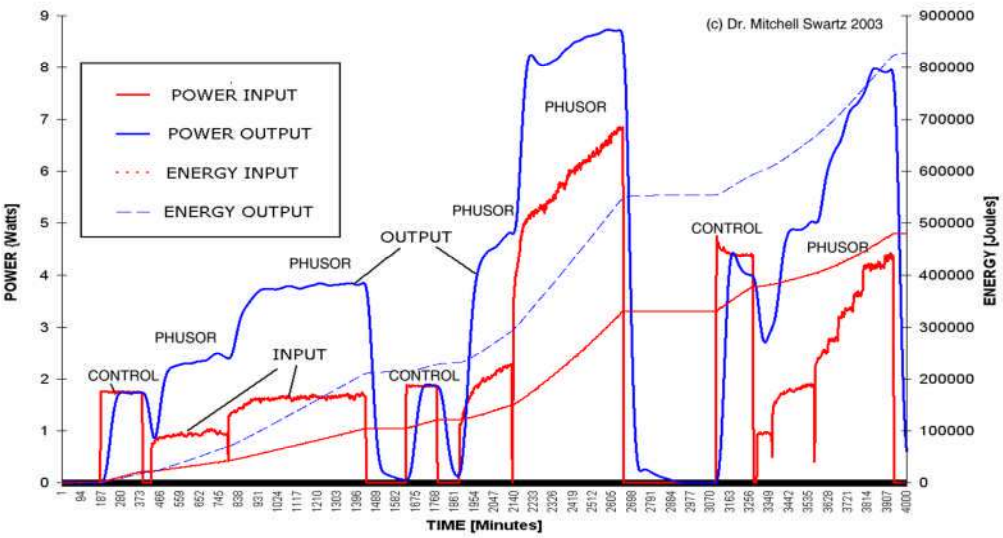

Figure 5: Input electrical power (solid red line) and output thermal power (solid blue line) of a single ohmic calorimeter as a function of time.

Figure 6 also has the integrated energy curves. It can be seen that for the ohmic joule (thermal) control that the integrated energies of the input and output arise in parallel. By contrast, in the deuterium-loaded heavy water systems, there is an expanding gap which is not parallel but which increases over time, corroborating that there has been excess heat generated; more than 50,000 joules compared to the control. It can be seen in Figure 6 that the observed output power is much greater for the deuteron-loaded system compared to the control and thus, there is excess heat.

5.2 - SIX WAYS TO CONFIRM OF EXCESS ENERGY IN LANR

Over the years, we have added increasing numbers of ancillary sensors, in situ cameras, and parallel computational systems to create redundant measurement of "excess heat". The experiments described in this paper involve examination of that putative excess energy five to six different ways. These methods include traceable NIST-calibrated heat flow sensors, and

paired Stirling engines. Outside of the core, paired NIST-calibrated heat flow sensors were used. In addition, the final heat output was ported to one of two paired Stirling engines (Figure 1), each also containing temperature measurement devices so they their own calorimetry was monitored. Figure 1 shows Stirling engines on outflow of LANR and ohmic control systems. The thermal driving cores, the heat flow sensors, the electricity conversion system, and other ducting on the way to the paired LANR-driven and ohmic control-drive Stirling engines lie within.

As an ohmic control, a 7.2 kilohm resistor, with additional insulation wraps protecting it, was used in the core. The electric current was supplied by a Keithley 225 current source; electric voltage was supplied by a HP Harrison Power supply. The system was electrically driven through a JET 10K Driver (2). The total experimental run time shown is 89 hours, with the LANR device run time being 60 hours. The maximum electric current was 8.6 mA. The peak electrical power in, P_{in}(max), was ~1.098 watts. The total electrical energy in, E_{in}, was ~192.3 kilojoules. The solution electrical resistance ranged from circa 25,000 to 15,000 ohms. The V_{oc} of the Pd Phusor at the end of the run was ~1.83 volts.

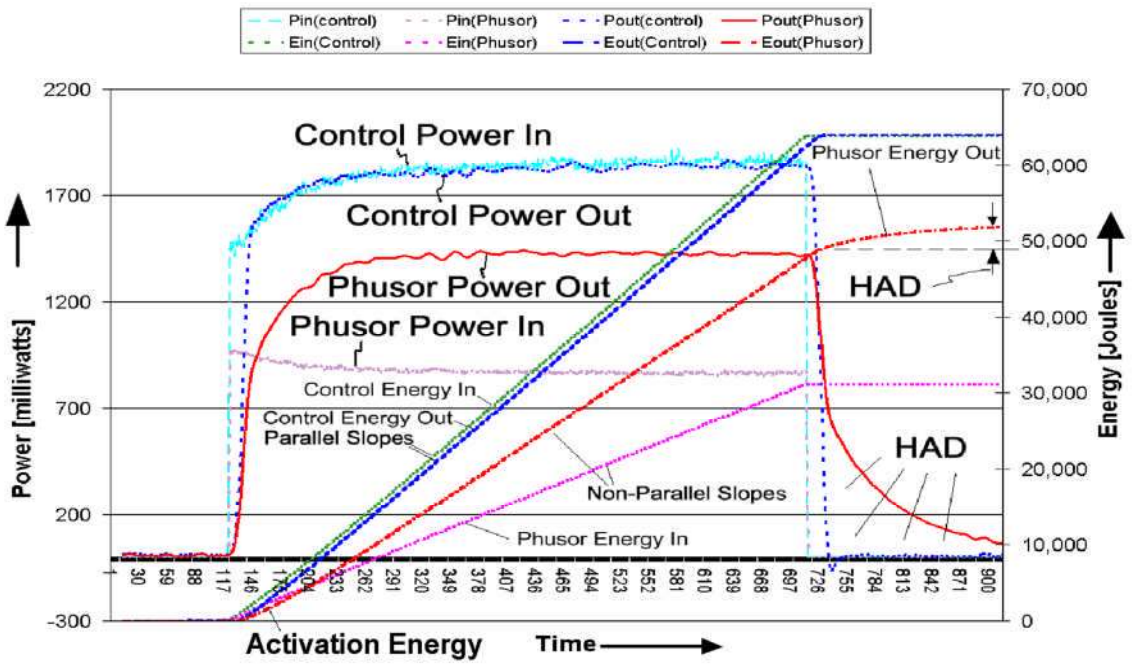

Figure 6: Input electrical power (solid red line) and output thermal power (solid blue line) as a function of time for a Dual Ohmic Control (DOC) Calorimeter showing and activation energy, power gain, excess heat, and "heat after death" (HAD).

Figures 7, 8, 9 and 10 show the results for a palladium (Ti-coupled) Phusor®-type cathode in D_2O vs. Pt as the anode. Figures 7 through 9 are from Run 34/35, E60912-16AB. Figure 7 shows the input and output powers and energies for both of the paired Stirling-engine calorimetric monitored systems driven by the Pd(Ti) Phusor and the ohmic control. Figure 8 shows the input-power-normalized (IPN) heat flows from both the Pd(Ti) Phusor and the ohmic

control. Figures 7 and 8 were obtained with the Stirling engines fixed in position. Figures 8 and 9 were obtained with the Stirling engines free to rotate. Figure 9 shows that Conservation of Energy is maintained in this system. Figure 10 is the OOP manifold of the system.

Figure 7 shows the input-power-normalized (IPN) delta-T (incremental temperature increase) for both the Pd(Ti) Phusor and the ohmic control. Excess power and energy are seen in the LANR curves because of the incremental distances between the output and input electrical powers and energies. In contrast, the control curves for power and energy significantly overlay each other.

These are the results of the six methods of excess power gain and excess heat determination for the engine-coupled Pd(Ti)/D_2O/Pt Phusor LANR device. The final determination of this run was made on calculation of the excess energy, HAD, and loading energies was based upon time integration, and the multiring calorimetry in the thermal waveform reconstruction method. The loading energy, an activation energy, for the prepared device in this run was 142 Joules. The HAD energy created after the run was 12.9 kilojoules.

This group of experiments proved that LANR-driven propulsion is more efficient that a similar propulsion system driven by an ohmic heater at the same power level. With LANR-driven heat, the increased efficiency led to mechanical rotation for days at lower input electrical power levels than that to the ohmic controls.

- Calculation of Power Gain by Method #1: The electrical power gain, P_{gain}, determined by input-power-normalized delta-T's, was 189% maximum, average for the entire run, 120%.
- Calculation of Power Gain by Method #2: The electrical power gain, P_{gain}, determined by input-power-normalized heat flow sensors, was 238% , with a minimum of 166%.
- Calculation of Power Gain by Method #3: The electrical power gain, P_{gain}, determined by maximum area correlated input-power-normalized heat flow, was 155%.
- Calculation of Power Gain by Method #4: The electrical power gain, P_{gain}, determined by input-power-normalized delta-T at the paired Stirling engines, was 159%.
- Calculation of Power Gain by Method #5: The electrical power gain, P_{gain}, determined by time-integrated multiring calorimetry with full waveform reconstruction analysis, was 142%. The excess energy was 41,528 Joules. The energy gain was ~142%.
- Calculation of Power Gain by Method #6: The electrical power gain, P_{gain}, determined by time-integrated multiring calorimetry with heat flow as the controlling input signal was 181%.

In summary, the input power normalized delta-measurement of the LANR device and the controls confirm that there was excess heat. The input power normalized heat flow measurements confirm that there was excess heat. The thermal waveform reconstruction calorimetriy confirm that there was excess heat.

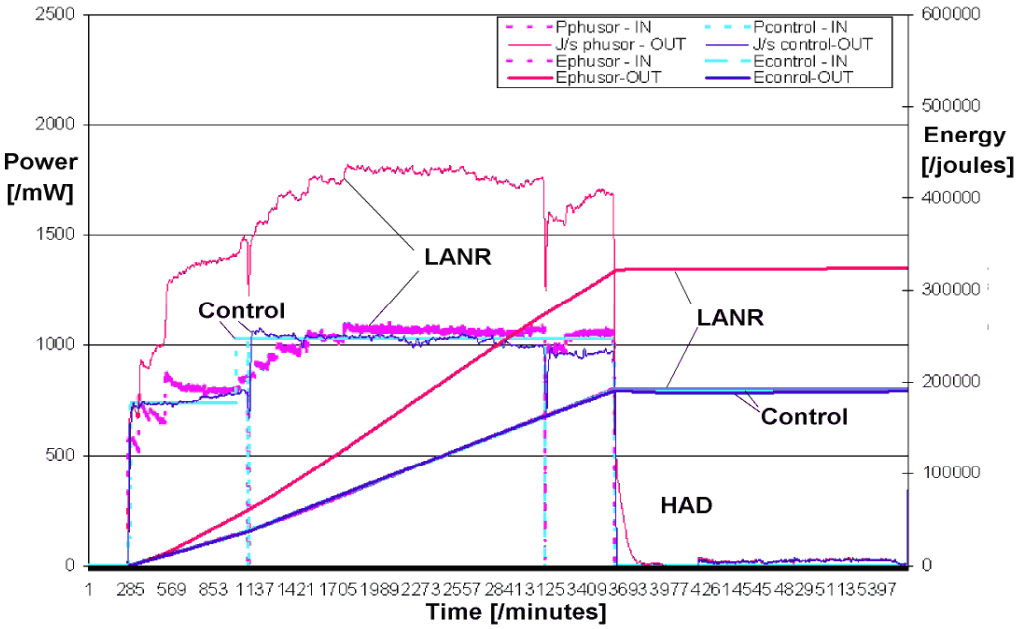

Figure 7 - Input and output powers and energies for paired Stirling-engine calorimetric monitored systems driven by Pd(Ti) Phusor and the ohmic control.

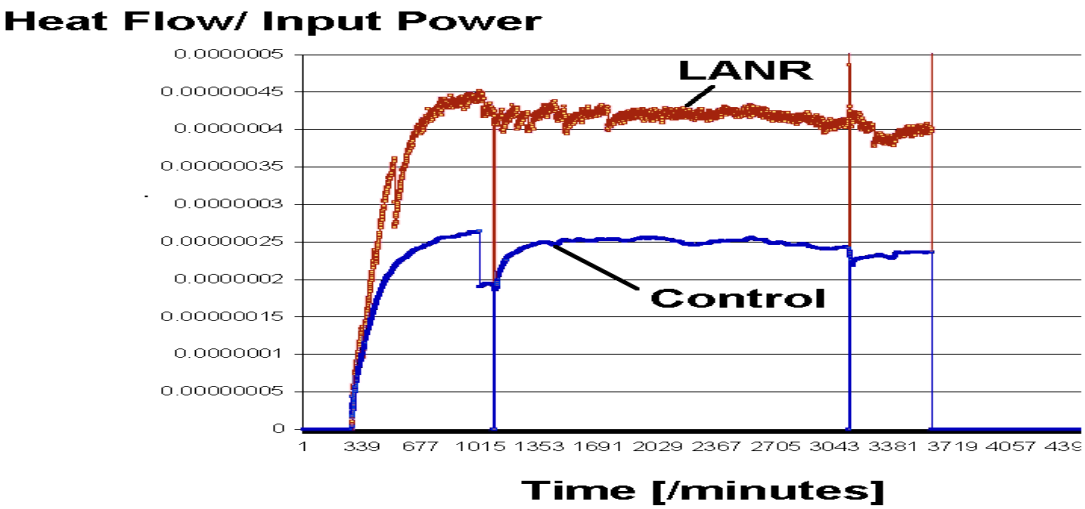

Figure 8 - Input-power-normalized heat flows from Pd(Ti) Phusor and ohmic control.

5.3 - Loss of Overunity at the Core as Energy goes to Motor

Figure 9 is an important critical graph which demonstrates that the over-unity performance (driven by D -> He^4 from the LANR) disappears entirely when the Stirling motor is allowed to rotate and remove heat from the system. The divergence of energy is zero. The removal of the energy from the core, through the heat flow sensors and the electricity producing sensors, to the propulsive Stirling engines is a zero sum "game" in that incremental excess energy has now been used, in the motor, and is now gone. "Excess" energy is conserved between compartments.

The removal of apparent excess heat when the LANR-driven motor demonstrated motion (energy dissipation, too) confirm that there was excess heat.

Furthermore, one of the more important conclusions is that the final possibility that the measurement of over-unity performance in this LANR system results from systematic instrument error is now zero, based upon this finding in Figure 9.

5.4 - Summary of LANR-Motor Systems Phase I-II

Our LANR-driven Stirling engine experiments with ohmic controls, and time-integration began in 2003. In those preliminary experiments, eleven runs were made using JET Pd and Ni Phusor®-type cathodes in matched Stirling engines. These runs proved that there could be direct conversion of deuterons to helium-4 over weeks producing motion without electricity or noxious emissions. In those runs, the LANR systems had a calorimetrically measured average gain of 170 +/- 22%. Using time-integration, the power gain was 152 +/-31%. The average input power for all engine runs $<P_{in}>$ was 3.6 watts. The average output LANR power for all runs $<P_{out}>$ was 4.5 watt. There was also Stirling engine motion on the LANR-Phusor side.

5.5 - Summary of of LANR-Motor Systems Phase III-IV

Phase IV of our LANR-driven Stirling engine experiments ended in 2008. In these runs, dual LANR-driven Stirling engine calorimeters with separate IPN(input power normalized) core temperature and delta-T monitoring, IPN heat flux measurement, IPN electric output, multiring calorimetry yielding thermal power spectrograms, and additional measurements at engines, were used. With this improved calorimetry, and improved enclosures and coupling, the LANR-driven motors had excess power gains of ~180-220%, with ~130% at 23 watts input electrical power.

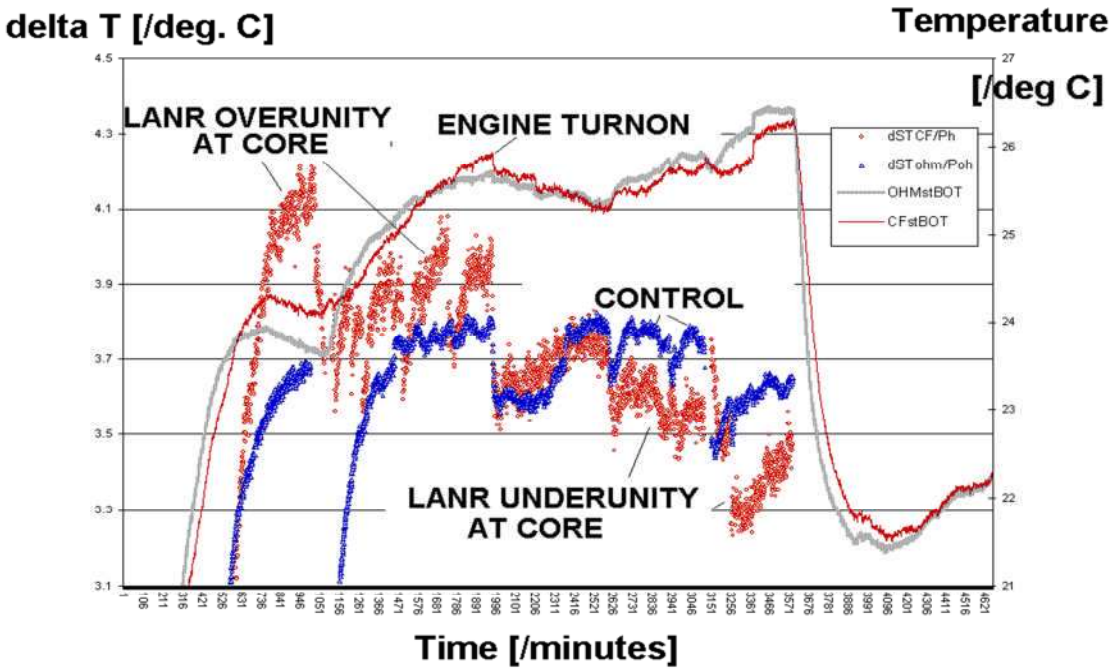

Figure 9 - Input-power-normalized delta-T increase for Pd(Ti) Phusor and ohmic control.

In the run of which the video was shown at ICCF-14, the LANR-driven Stirling engine went, based on the rotational circumference but without any additional traction or restraining force, an equivalent 11.6 miles vs. 0.0 for the ohmic control driven engine. The power gain curves showed the characteristic optimal operating point and OOP manifold (Figure 10).

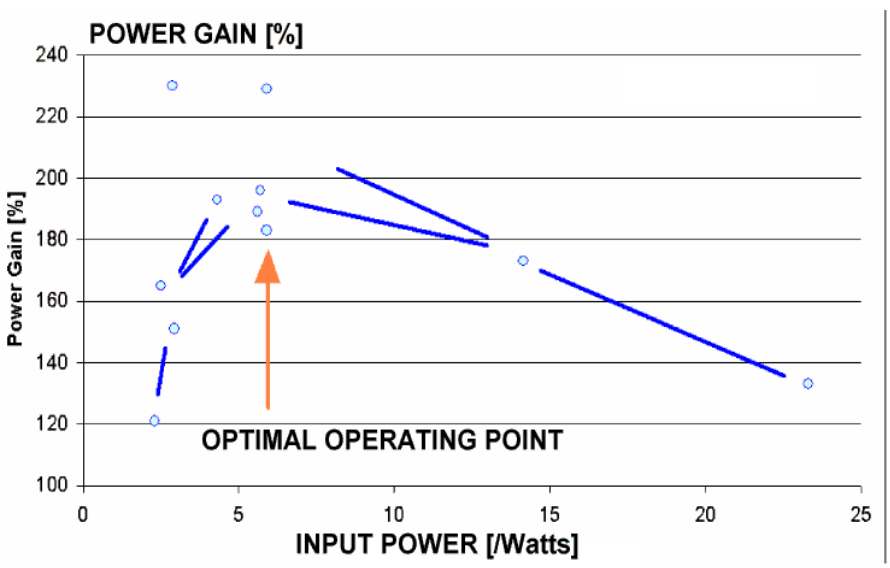

Figure 10 - Optimal operating point and OOP manifold for LANR-driven Stirling engine.

Table 1 -SUMMARY EXCESS HEAT OBSERVED at JET Energy, Inc.

PALLADIUM HEAVY WATER (PdD) SYSTEM

- Excess energy significant after full loading and early processing; depends upon loading rate, flux, purity, contamination, confinement time, and operating point.
- Peak excess power: 0.5 to 15 watts (occasionally higher)
- Activation energy ~ 60.7 kilojoules/mole.
- Activity quenched by many things.
- Critical input electrical current density 1.5 +/- 0.3 milliamperes/cm^2
- May exist threshold voltages before adequate loading is achieved.
- Open Circuit Voltage: 2.4 volts heralds good activity [ICCF-10 '03]

Power Gain $Pd/D_2O/Pt$ (all)	0.4 – 3.4
Power Gain [$Pd/D_2O/Pt$] LANR Systems	0.4-2.3 [ICCF-10 '03]
Power Gain [$Pd/D_2O/Au$] Phusor®	1.5-2.7 [ICCF-10 '03]
Power Gain [$Pd/D_2O/Au$] Phusor®	1.5- 8.0 [MIT Adv Coll. '05]
Power Gain [$Pd/D_2O/Pt$] with Stirling Engines	1.5-1.92 [ICCF-14 '08]
Power Gain [$Pd(Ti)/D_2O/Pt$] with Stirling Engines	1.8-2.2 [ICCF-14 '08]

ENERGY GAIN BASED UPON LANR-DRIVEN STIRLING ENGINES

Peak Power Gain (Phase I-II)	1.7	[ICCF-14 '08]
Peak Power Gain (Phase III-IV)	1.8 - 2.2	[ICCF-14 '08]
Time-integrated Energy Gain (Phase I-II)	1.52	[ICCF-14 '08]

EXCESS HEAT OBSERVED IN Pd D_2O CODEPOSITIONAL SYSTEM

- Codeposition 8.2 mM $PdCl_2$ OOP maturation effect
- Codeposition 3-100 mM $Pd(OD)_2$ Pt improved output [ICCF-10 '03]
- DAP Codeposition $Pd/Pd(OD)_2/Pd$-Au highest power gain, ephemeral endurance

Peak Power Gain [Pd/D_2O,$Pd(OD)_2$/Pt,Au] DAP Phusor® ~80 [ICCF-14 '08]

EXCESS HEAT OBSERVED IN SOME NICKEL LIGHT WATER SYSTEMS

- Excess energy significant for some samples for a limited period of time
- Damaged by high current and D_2O

Power Gain labile with elec. conduct change Ni/H_2O_{1-x},D_2O_x/Pt [Swartz ICCF-11]

- Peak Excess Volume Power Density 7.0 watts/cm^3

Power Gain $Ni/H_2O/Pt$	1.3 - ~3 Ni Phusor	[Swartz Fusion Technology '97]
Power Gain $Ni/H_2O/Pt$	1.1 - ~2.4	[Swartz Fusion Technology '97]
Power Gain $Ni/H_2O/Ni$	0.96 - 2.1	
Power Gain $Ni/H_2O/Au$	2 - 5 Ni Phusor	[Swartz Fusion Technology '99]

EXCESS HEAT <u>NOT</u> OBSERVED IN IRON, ALUMINUM, DAMAGED NICKEL

Excess heat <u>NOT</u> seen with Iron, Aluminum, or damaged Nickel(*) as Cathodes

Power "Gain"	$Al/H_2O/Pt$	0.7 – 0.8
Power "Gain"	$Fe/H_2O/Fe$	0.61 – 0.79

INFREQUENT IRREGULAR VERY LOW LEVEL BORDERLINE EXCESS HEAT OBSERVED in CONTAMINATED Au, Pd, Ni, Pt , Alloy CATHODES

Power Gain 0.73 – 1.19 [Swartz LENR-2 1996]

6. - LANR Technology – Advanced Apps Around the Corner

LANR will become an energy multiplier because the energy density of LANR reactions is ten million times that of gasoline. At ICCF-14, JET Energy, Inc. reported on thermal and efficiency issues of the electrical feedback loop, and our preliminary results concerning LANR-driven Stirling engines. Given the prevalence of the fuel, and the incredible efficiency, LANR will play a critical role in all future technologies with potential revolutionary applications to all energy issues---robotics, transportation, electricity production, space travel. Larger LANR power devices will fit into a hybrid car and offer methods to power in vivo medical devices such as the artificial heart.

Acknowledgments

The author thanks Gayle Verner for her meticulous help in manuscript and idea development, and also Jeffrey Tolleson, Alex Frank, Alan Weinberg, Allen Swartz, Brian Josephson, Brian Ahern, Jeff Driscoll, Isidor Straus, Michael Beigel, Steven Olasky, Raymond Kurzweil, Aaron Kleiner, Glen Dash, Charles Entenmann, Frank Gordon, Larry Forsley, Pamela Mosier-Boss, Scott Chubb, Peter Hagelstein, Robert Smith, Richard Kramer for their helpful conversations, and JET Energy and New Energy Foundation for their additional support. PHUSOR® is a registered trademark of JET Energy, Incorporated. PHUSOR®-technology is protected by U.S. Patents D596724, D413659 and Patents pending.

REFERENCES

1. Swartz, M., "Consistency of the Biphasic Nature of Excess Enthalpy in Solid State Anomalous Phenomena with the Quasi-1-Dimensional Model of Isotope Loading into a Material", Fusion Technology, 31, 63-74 (1997).
2. Swartz, M., G. Verner, "Excess Heat from Low Electrical Conductivity Heavy Water Spiral-Wound Pd/D2O/Pt and Pd/D2O-PdCl2/Pt Devices", Condensed Matter Nuclear Science, Proceedings of ICCF-10, eds. P.L.Hagelstein, S.Chubb, World Scientific Publishing, NJ, ISBN 981-256-564-6, 29-44; 45-54 (2006).
3. Swartz, M, "Improved Electrolytic Reactor Performance Using pi-Notch System Operation and Gold Anodes, Trans. American Nuclear Association, Nashville, Tenn Meeting, (ISSN:0003-018X publisher LaGrange, Ill) 78, 84-85 (1998) .
4. Swartz, M., "Patterns of Failure in Cold Fusion Experiments", Proc. 33RD Intersociety Engineering Conference on Energy Conversion, IECEC-98-I229, CO, Aug.(1998).
5. Swartz, M., G. Verner, "Dual Ohmic Controls Improve Understanding of 'Heat after Death'", Transactions American Nuclear Society, vol. 93, ISSN:0003-018X, 891-892 (2005).
6. Swartz. M., "The Impact of Heavy Water (D2O) on Nickel-Light Water LANR Systems", Proc. ICCF-9, 335-342.
7. Swartz, M., G. Verner, "Metamaterial Function of Cathodes Producing Hydrogen Energy and Deuteron Flux", Proceedings of the 14th International Conference on Condensed Matter Nuclear Science (2010).
8. Swartz, M., G. Verner, "Photoinduced Excess Heat from Laser-Irradiated Electrically-Polarized Palladium Cathodes in D2O", Condensed Matter Nuclear Science, Proc.

ICCF-10, eds. Peter L. Hagelstein, Scott Chubb, NJ, ISBN 981-256-564-6, 213-226 (2006).
9. Swartz, M., "Codeposition Of Palladium And Deuterium", Fusion Technology, 32, 126-130 (1997).
10. Swartz, M., G.Verner, A.Weinberg, “Non-Thermal Near-IR Emission Linked with Excess Power Gain in LANR Devices”, Proceedings of the 14th International Conference on Condensed Matter Nuclear Science (2010).
11. Swartz, M., "Noise Measurement in cold fusion systems, Journal of New Energy, 2, 2, 56-61 (1997)
12. Arata, Y. Y.C. Zhang, 'Anomalous Production of Gaseous 4He at the Inside of DS-Cathode During D2-Electrolysis', Proc. Jpn. Acad. Ser. B, Vol. 75, p. 281 (1999); Arata, Y. and Y.C. Zhang, Observation of Anomalous Heat Release and Helium-4 Production from Highly Deuterated Fine Particles. Jpn. J. Appl. Phys. Part 2, 1999. 38: p. L774; Arata, Y. and Y. Zhang, The Establishment of Solid Nuclear Fusion Reactor. J. High Temp. Soc., 2008. 34(2): p. 85.
13. Case, L.C. Catalytic Fusion of Deuterium into Helium-4. in The Seventh International Conference on Cold Fusion., Vancouver, Canada: ENECO, Inc., Salt Lake City, UT. (1998).
14. Dardik, I., H. Branover, A. El-Boher, D. Gazit, E. Golbreich, E. Greenspan, A. Kapusta, B. Khachatorov, V. Krakov, S. Lesin, B. Michailovitch, G. Shani, and T. Zilov, 'Intensification of Low Energy Nuclear Reactions Using Superwave Excitation', Proceedings of the 10th International Conference on Cold Fusion (2003).
15. Dash, J. and D.S. Silver. Surface Studies After Loading Metals With Hydrogen And/Or Deuterium, 13th Conf. CMNS 2007. Sochi, Russia; Dash, J. and S. Miguet, Microanalysis of Pd Cathodes after Electrolysis in Aqueous Acids. J. New Energy, 1996. 1(1): p. 23.
16. Fleischmann, M., S. Pons, "Electrochemically Induced Nuclear Fusion of Deuterium", J. Electroanal. Chem., 261, 301-308, erratum, 263, 187 (1989); M. Fleischmann, S. Pons, "Some comments on the paper Analysis of Experiments on Calorimetry of LiOD/D2O Electrochemical Cells, R.H.Wilson et al., J. Electroanal. Chem., 332 (1992) 1* ", J. Electroanal. Chem., 332, 33-53, (1992); M. Fleischmann, S. Pons, "Calorimetry of the Pd-D2O system: from simplicity via complications to simplicity", Physics Letters A, 176, 118-129, (1993); M. Fleischmann, S. Pons, M. Anderson, L.J. Li, M. Hawkins, "Calorimetry of the palladium-deuterium-heavy water System", Electroanal. Chem., 287, 293, (1990)
17. Iwamura, Y., M. Sakano, and T. Itoh, Elemental Analysis of Pd Complexes: Effects of D2 Gas Permeation. Jpn. J. Appl. Phys. A, 2002. 41: p. 4642; Iwamura, Y., et al., "Observation Of Surface Distribution Of Products By X-Ray Fluorescence Spectrometry During D2 Gas Permeation Through Pd Complexes", in The 12th International Conference on Condensed Matter Nuclear Science. 2005. Yokohama, Japan.
18. Letts D., D. Cravens, "Laser Stimulation of Deuterated Palladium: Past and Present", Proceedings of the 10th International Conference on Cold Fusion (2003).

19. Letts, D. and P.L. Hagelstein. Stimulation of Optical Phonons in Deuterated Palladium. in ICCF-14 International Conference on Condensed Matter Nuclear Science. 2008. Washington, DC.; Letts, D., D. Cravens, and P.L. Hagelstein, Thermal Changes in Palladium Deuteride Induced by Laser Beat Frequencies, in Low-Energy Nuclear Reactions Sourcebook, J. Marwan and S. Krivit, Editors. 2008,
20. McKubre, M., F. Tanzella, P. Hagelstein, K. Mullican, and M. Trevithick, 'The Need for Triggering in Cold Fusion Reactions,' Proc. 10th International Conf. on Cold Fusion (2003).
21. Miles, M.H., R.A. Hollins, B.F.Bush, J.J. Lagowski, R.E. Miles, "Correlation of excess power and helium production during D2O and H2O electrolysis", J. Electroanal. Chem., 346 (1993) 99-117.
22. Miles, M.H., B.F.Bush, "Heat and Helium Measurements in Deuterated Palladium", Transactions of Fusion Technology, vol 26, Dec. 1994, pp 156-159.
23. Miles, M.H., et alia, "Calorimetric Analysis of a Heavy Water Electrolysis Experiment Using a Pd-B Alloy Cathode", Naval Research Laboratory Report NRL/MR/6320-01-8526, 155 pp. (March 16, 2001).
24. Miley, G.H., G. Narne, T. Woo, Use of combined NAA and SIMS analyses for impurity level isotope detection. J. Radioanal. Nucl. Chem., 2005. 263(3): p. 691-696; Miley, G.H. and J. Shrestha, Transmutation Reactions and Associated LENR Effects in Solids, in Low-Energy Nuclear Reactions Sourcebook, J. Marwan and S. Krivit, Editors. 2008, Oxford University Press.
25. Mosier-Boss, P.A. and S. Szpak, 'The Pd/nH System: Transport Processes and Development of Thermal Instabilities', Il Nuovo Cimento, Vol. 112A, pp. 577-585 (1999).
26. Mosier-Boss, P.A, S. Szpak, F.E. Gordon, and L.P.G. Forsley, 'Use of CR-39 in Pd/D Co-Deposition Experiments', European Physics Journal-Applied Physics, Vol. 40, pp. 293-303 (2007).
27. Mosier-Boss, P.A., S. Szpak, F.E. Gordon, and L.P.G. Forsley, 'Triple Tracks in CR-39 as the Result of Pd-D Co-deposition: Evidence of Energetic Neutrons,' Naturwissenschaften, in press.
28. Pons, S., Fleischmann, M., "Heat After Death," Proc. ICCF-4, Maui, EPRI TR104188-V2, vol. 2, 8-1 (1994); Trans. Fusion Technology, 26, Number 4T, Part 2, p. 87 (December 1994).
29. Srinivasan, M., et alia., "Tritium and Excess Heat Generation During Electrolysis of Aqueous Solutions of Alkali Salts with Nickel Cathode," Frontiers of Cold Fusion, Ed. by H. Ikegami, Proceedings of the Third International Conference on Cold Fusion, October 21-25, 1992, Universal Academy Press, Tokyo, pp 123-138.
30. Stringham, R., Cavitation and Fusion, ICCF-10. 2003. Cambridge, MA
31. Szpak S., P.A. Mosier-Boss, C. Young, and F.E. Gordon, 'Evidence of Nuclear Reactions in the Pd Lattice', Naturwissenschaften, Vol. 92, pp. 394-397 (2005).
32. Szpak S., P.A. Mosier-Boss, and J.J. Smith, 'On the Behavior of Pd Deposited in the Presence of Evolving Deuterium', J. Electroanal. Chem., Vol. 302, pp. 255-260 (1991).
33. Szpak S., P.A. Mosier-Boss, S.R. Scharber, and J.J. Smith, 'Charging of the Pd/nH System: Role of the Interphase', J. Electroanal. Chem., Vol. 337, pp. 147-163 (1992).

34. Szpak S., P.A. Mosier-Boss, and J.J. Smith, 'Deuterium Uptake During Pd-D Codeposition', J. Electroanal. Chem., Vol. 379, pp. 121-127 (1994).
35. Szpak S., P.A. Mosier-Boss, M.H. Miles, and M. Fleischmann, 'Thermal Behavior of Polarized Pd/D Electrodes Prepared by Co-Deposition', Thermochim. Acta, Vol. 410, pp. 101-107 (2004).
36. Szpak S., P.A. Mosier-Boss, S.R. Scharber, and J.J. Smith, 'Cyclic Voltammetry of Pd+D Codeposition', J. Electroanal. Chem., Vol. 380, pp. 1-6 (1995).
37. Szpak S. and P.A. Mosier-Boss, 'On the Behavior of the Cathodically Polarized Pd/D System: a Response to Vigier's Comments', Phys. Letts. A, Vol. 221, pp. 141-143 (1996).
38. Szpak S., P.A. Mosier-Boss, R.D. Boss, and J.J. Smith, 'On the Behavior of the Pd/D System: Evidence for Tritium Production', Fusion Technology, Vol. 33, pp. 38-51 (1998).
39. Szpak S., P.A. Mosier-Boss, and J.J. Smith, 'On the Behavior of the Cathodically Polarized Pd/D System: Search for Emanating Radiation', Phys. Letts. A, Vol. 210, pp. 382-390 (1996).
40. Szpak S., P.A. Mosier-Boss, and F.E. Gordon, 'Further Evidence of Nuclear Reactions in the Pd/D Lattice: Emission of Charged Particles', Naturwissenschaften, Vol. 94, pp. 511-514 (2007).
41. Szpak, S., et al., The effect of an external electric field on surface morphology of co-deposited Pd/D films. J. Electroanal. Chem., 580: 284-290, (2005).
42. Violante, V., E. Castagna, C. Sibilia, S. Paoloni, and F. Sarto, 'Analysis of Mi-Hydride Thin Film After Surface Plasmons Generation by Laser Technique' ' Proceedings of the 10th International Conference on Cold Fusion (2003).
43. Will, F.G., K. Cedzynska, D.C. Linton, "Tritium Generation in Palladium Cathodes with High Deuterium Loading", Transactions of Fusion Technology, vol 26, Dec. 1994, pp 209-213; "Reproducible tritium generation in electrochemical cells employing palladium cathodes with high deuterium loading", J. Electroanal. Chem 360 (1993) 161-176.
44. Swartz. M., "Patterns of Success in Research Involving Low-Energy Nuclear Reactions", Infinite Energy, 31, 46-48, (2000).
45. Hagelstein, P.L., et al. A Theoretical Formulation for Problems in Condensed Matter Nuclear Science. in ICCF-14 International Conference on Condensed Matter Nuclear Science. 2008. Washington, DC.; Hagelstein, P.L. and I. Chaudhary, Models Relevant to Excess Heat Production in Fleischmann-Pons Experiments, in Low-Energy Nuclear Reactions Sourcebook, J. Marwan and S. Krivit, Editors. 2008, Oxford University Press.
46. Rabinowitz, M., et al. Opposition and Support for Cold Fusion. in Fourth International Conference on Cold Fusion, Lahaina, Maui: Electric Power Research Institute 3412 Hillview Ave., Palo Alto, CA 94304, (1993).
47. Li, X.Z., et al. The Precursor of "Cold Fusion" Phenomenon in Deuterium/Solid Systems. in Anomalous Nuclear Effects in Deuterium/Solid Systems, "AIP Conference Proceedings 228". 1990. Brigham Young Univ., Provo, UT: American Institute of Physics, New York.

48. Takahashi, A. and N. Yabuuchi, Study on 4D/TSC Condensation Motion by Non-Linear Langevin Equation, in Low-Energy Nuclear Reactions Sourcebook, J. Marwan and S. Krivit, Editors. 2008, Oxford University Press; Takahashi, A. Dynamic Mechanism of TSC Condensation Motion. in ICCF-14 International Conference on Condensed Matter Nuclear Science. 2008. Washington, DC.
49. Swartz, M., "Possible Deuterium Production From Light Water Excess Enthalpy Experiments using Nickel Cathodes", Journal of New Energy, 3, 68-80 (1996).
50. Swartz, M., "Phusons in Nuclear Reactions in Solids", Fusion Technology, 31, 228-236 (1997).
51. Chubb, S.R. and T.A. Chubb, The Role of Hydrogen Ion Band States in Cold Fusion. Trans. Fusion Technol., 26(4T), 414.(1994);
52. Chubb, T.A., S.R.Chubb, "Ion Band States: What they are, and How they Affect Cold Fusion", Cold Fusion Source Book, ibid., 75, (1994).
53. Papaconstantopoulos, D.A., B.M. Klein, et alia, "Band structure and superconductivity of PdDx and PdHx", Physical Review, 17, 1, 141150, (1977).
54. Wicke, E., H. Brodowsky, "Hydrogen in Palladium and Palladium Alloys", Hydrogen in Metals II, G. Alefield, J. Volkl, Eds., Springer, Berlin (1978).
55. Teichler, H., "Theory of hydrogen hopping dynamics including hydrogen-lattice correlations", J. Less-Common Metals, 172-174 (1991) 548-556.
56. Klein, B.M., R. E. Cohen, "Anharmonicity and the inverse isotope effect in the palladium-hydrogen system", Phys. Rev. B, 45, 21, 405 (1992).
57. Bussard, R.W., "Virtual-State Internal Nuclear fusion in Metal Lattices", Fusion Technology, 16, 231-236 (1989).
58. Gibb, T.C., "Principles of Mossbauer Spectroscopy", Chapman and Hall, London (1974).
59. Dickson, D.P.E., Berry, F., "Mossbauer Spectroscopy", Cambridge University Press (1983).
60. Gonser, U., "Mossbauer Spectroscopy", Springer-Verlag, NY (1975).
61. Swartz, M, G. Verner, "Bremsstrahlung in Hot and Cold Fusion", J New Energy, 3, 4, 90-101 (1999)
62. Swartz. M., Three Physical Regions of Anomalous Activity in Deuterided Palladium, Infinite Energy, Vol. 14, Issue 61, 19-31 (2008).
63. Swartz. M., "Catastrophic Active Medium Hypothesis of Cold Fusion" Vol. 4. "Proceedings: "Fourth International Conference on Cold Fusion" sponsored by EPRI and the Office of Naval Research (1994); Swartz, M., "Hydrogen Redistribution By Catastrophic Desorption In Select Transition Metals", Journal of New Energy, 1, 4, 26-33 (1997)
64. Swartz, M., "Quasi-One-Dimensional Model of Electrochemical Loading of Isotopic Fuel into a Metal", Fusion Technology, 22, 2, 296-300 (1992).
65. Swartz, M., "Isotopic Fuel Loading Coupled to Reactions At an Electrode", Fusion Technology, 26, 4T, 74-77 (1994).
66. Swartz, M, "Optimal Operating Point Characteristics of Nickel Light Water Experiments", Proc. ICCF-7 (1998).
67. Swartz, M., "Generality of Optimal Operating Point Behavior in Low Energy Nuclear Systems", Journal of New Energy, 4, 2, 218-228 (1999).

68. Swartz. M., P.L.Hagelstein, G. Verner, K. Wright, "Transient Vacancy Phase States in Palladium following high dose rate Electron Beam Irradiation", Journal of New Energy, (2003).
69. Bass, R.W., M.R.Swartz, “Empirical System Identification (ESID) and Optimal Control of Lattice-Assisted Nuclear Reactors”, Proceedings of the 14th International Conference on Condensed Matter Nuclear Science (2010).
70. Swartz, M, L.Forsley, Analysis of "Superwave-as-Transitory-OOP-Peak" Hypothesis Proceedings of the 14th International Conference on Condensed Matter Nuclear Science (2010).
71. Swartz, M., "Thermal Conduction and Non-differential Temperature Corrections to the Enthalpic Flow Equation", Journal of New Energy, 3, 1, 10-13, (1998).